Journal of Power Sources 248 (2014) 1105–1117

Contents lists available at ScienceDirect

Journal of Power Sources

journal homepage: www.elsevier.com/locate/jpowsour

The electrochemical reactions of pure indium with Li and Na: Anomalous electrolyte decomposition, benefits of FEC additive, phase transitions and electrode performance

Samantha A. Webb [a], Loïc Baggetto [a,*], Craig A. Bridges [b], Gabriel M. Veith [a,*]

[a] Materials Science and Technology Division, Oak Ridge National Laboratory, 1 Bethel Valley Road, Oak Ridge, TN 37831, USA
[b] Chemical Sciences Division, Oak Ridge National Laboratory, Oak Ridge, TN 37831, USA

HIGHLIGHTS

- Indium thin films are evaluated as anode for Li-ion and Na-ion batteries.
- Anomalous electrolyte decomposition and benefits of FEC additive are investigated.
- High storage capacity (950 mAh g^{-1}) and good retention obtained for Li with FEC.
- Limited storage capacity (125 mAh g^{-1}) for Na.
- Excellent rate capability with 950 mAh g^{-1} retained at 10 C for Li.

GRAPHICAL ABSTRACT

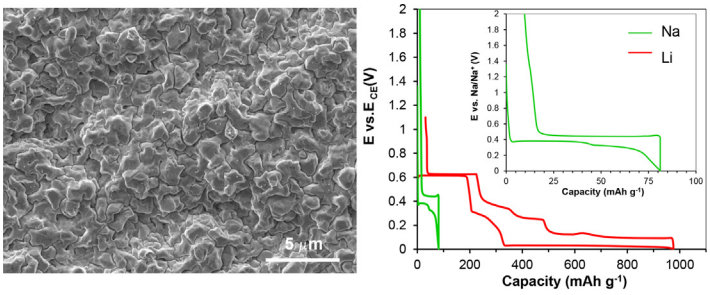

ARTICLE INFO

Article history:
Received 9 August 2013
Received in revised form
27 September 2013
Accepted 6 October 2013
Available online 23 October 2013

Keywords:
Indium (In) sputtered thin films
Lithium-ion anode
Sodium-ion anode
Anomalous electrolyte decomposition
Benefits of fluoroethylene additive (FEC) additive
Very high rate performance

ABSTRACT

Indium thin films were evaluated as an anode material for Li-ion and Na-ion batteries (theoretical capacities of 1012 mAh g^{-1} for Li and 467 mAh g^{-1} for Na). XRD data reveal that several known Li–In phases (LiIn, Li_3In_2, $LiIn_2$ and $Li_{13}In_3$) form providing 950 mAh g^{-1} reversible capacity. In contrast, the reaction with Na is severely limited (75–125 mAh g^{-1}). XRD data of short-circuited cells (40 h at 65 °C) show the coexistence of NaIn, In, and an unknown Na_xIn phase. In electrodes exhibit anomalous electrolyte decomposition characterized by large discharge plateaus at 1.4 V vs Li/Li^+ and 0.9 V vs Na/Na^+. The presence of 5 wt% fluoroethylene carbonate additive suppresses the occurrence of the electrolyte decomposition during the first cycle but does not necessarily prevent it upon further cycling. Prevention of the anomalous decomposition can be achieved by restricting the (dis)charge voltages, increasing the current or by using larger amounts of FEC. The native surface oxides (In_2O_3) are responsible for the pronounced electrolyte decomposition during the first cycle while other In^{3+} species are responsible during the subsequent cycles. We also show that indium electrodes can exhibit very high rate capability for both Li (100 C-rate) and Na (30 C-rate).

1. Introduction

With the growing interest in sodium-ion batteries, it is crucial to develop suitable anode materials to couple with the growing body of known Na-ion cathodes [1]. One of the challenges in developing suitable Na-ion anodes is the significantly different structures, chemistries, and reaction pathways which occur during the reaction with Na compared to Li [2–11]. Although the end compositions of Sn (847 mAh g^{-1}) and Sb (660 mAh g^{-1}) during the reactions with Li and Na are similar, $Na_{15}Sn_4$ and $Li_{21+5/16}Sn_5$ [2,3], and Na_3Sb and Li_3Sb [4,5], the crystallographic structures of the reaction intermediates and end members are

* Corresponding authors.
E-mail addresses: baggettol@ornl.gov (L. Baggetto), veithgm@ornl.gov (G. M. Veith).

0378-7753/$ – see front matter © 2013 Elsevier B.V. All rights reserved.
http://dx.doi.org/10.1016/j.jpowsour.2013.10.033

very different. Another striking example of such difference is Ge which can alloy up to $Li_{15}Ge_4$ with Li [6] but is restricted to an amorphous phase with a composition close to that of NaGe with Na [7]. Similarly, Si can alloy up to $Li_{15}Si_4$ [8,9] but the reaction of Si with Na has been predicted to be severely hindered [10,11], as we observed experimentally (not presented). Intermetallics based on, for example, Si, Sn and Sb have attracted a lot of attention for Li-ion batteries thanks to their better cycle-life and rate performance [9]. Our group, and others, have focused on exploring the suitability of Sn- and Sb-based intermetallic materials for the reaction with Na, such as Cu_6Sn_5 [12], AlSb [13], Cu_2Sb [14], Mo_3Sb_7 [15], and SnSb [16] to enhance the capacity retention and rate performance of the electrode material.

As part of this pursuit we are investigating indium based anodes. Indium ($Z = 49$) is a neighbor of Sn ($Z = 50$) and Sb ($Z = 51$) in the periodic table of elements, which may help us to understand the reaction chemistry of these elements. In addition, indium has large theoretical capacities with Li (1012 mAh g^{-1}, $Li_{13}In_3$) [17] and Na (467 mAh g^{-1}, Na_2In) [18], making it a potentially interesting anode material for both Li-ion and Na-ion batteries. For the Li–In system the intermetallics with known crystal structure are $Li_{0.3}In_{1.7}$, LiIn, Li_5In_4, Li_3In_2, Li_2In and $Li_{13}In_3$ [17]. For the Na–In system, crystal compounds $Na_{15}In_{27.4}$, $Na_7In_{11.6}$, NaIn and Na_2In have been reported [18]. Interestingly, Vaughey et al. suggested that the line compounds of the Li–In phase diagram may form during the electrochemical reaction of In with Li [19]. However, to the best of our knowledge, there is only one study of pure indium with Li [20]. This work was realized at high temperatures on a limited composition range with focus on the transport properties and did not discuss the phase transformations or the performance of indium at room temperature [20]. Other works have focused on the cubic zinc blende InSb material as a potential anode for Li-ion batteries with high capacity, and described the reaction mechanism using in situ XRD and in situ x-ray absorption spectroscopy [21–23]. These works, however, did not focus on the reaction of pure indium with Li. Other In-based anode materials have also shown some promising properties for Li-ion batteries, such as the oxide In_2O_3 [24] or the phosphide InP [25].

The present contribution investigates for the first time the fundamental electrochemical and structural properties of pure indium during the reactions with Li and Na. As we have recently demonstrated for various chemistries discussed above [2,4,6–8,12–15], the use of thin films is a powerful tool to elucidate the intrinsic properties of materials during electrochemical reactions. Galvanostatic cycling and quasi-equilibrium measurements using the galvanostatic intermittent titration technique (GITT) have been performed on thin film electrodes to determine the dynamic and quasi-equilibrium potential profiles, as well as to measure the maximum practical storage capacity of the electrode material. The data shows the anomalous decomposition of the carbonate electrolytes at relatively high voltages (1.4 V vs. Li/Li^+ and 0.9 V vs. Na/Na^+), which is well-known for Sn anodes during electrochemical reactions with Li and Na [2,3,26]. In addition, we demonstrate that the right amount of fluoroethylene carbonate (FEC) electrolyte additive and the use of appropriate cut-off voltages are essential to effectively suppress the electrolyte decomposition for both Li and Na electrolytes. In addition, the origins of the anomalous electrolyte decomposition are studied using Scanning Electron Microscopy (SEM) and X-ray Photoelectron Spectroscopy (XPS). Moreover, the reaction mechanism of indium with Li and Na thoroughly studied by *ex situ* XRD using Mo K_α radiation is presented. Finally, the electrode cycling and rate performances are presented, and failure mechanisms of cycled electrodes investigated post-mortem using SEM are discussed.

2. Experimental

Thin films were grown on roughened Cu foils by DC magnetron sputtering of a homemade indium target obtained by pressing indium shot (Alfa Aesar, 99.99%) into a 2″ diameter disc. Sputtering was conducted in Ar (99.9995%) plasma at 10 W power and 20 mTorr pressure using a chamber generally pumped down to a base pressure of 5×10^{-7} Torr. Thin films were weighed with 10 μg precision using Sartorius or Mettler balances. Film thickness was back-calculated based on an expected density of In (7.30 g cm^{-3}).

Electrochemical characterization was conducted at 25 °C inside a thermostated incubator using 2-electrode coin cells (2032 hardware, Hohsen) prepared inside an Ar-filled glovebox. The cells consisted of pure Na (Sigma–Aldrich) or Li (Alfa Aesar) as counter electrodes, glass fiber separators impregnated by 1 M $NaClO_4$ in anhydrous PC (Sigma–Aldrich) or 1.2 M $LiPF_6$ in dimethyl carbonate (DMC) and ethylene carbonate (EC) (Novolyte) electrolyte solutions, and In thin films as working electrodes. Unless specified otherwise, 5 wt% of anhydrous FEC (Sigma–Aldrich) was added to the electrolytes. Constant current (CC) and constant voltage (CV) cycling was performed on a Maccor 4000 series for electrodes with a surface area of 0.97 cm^2. 1 C-rate current corresponds to the current required to (dis)charge the electrodes in 1 h. GITT profiles were measured with rest periods of 2 h.

XPS measurements were conducted on PHI 3056 spectrometer equipped with Al K_α source (1486.6 eV) operated at pressures below 10^{-8} Torr. Samples were loaded into the XPS chamber with an air-tight vacuum transfer system after rinsing with anhydrous DMC (Sigma–Aldrich). High resolution scans were acquired at 350 W, 23.5 eV constant pass energy, and 0.05 eV energy step, and survey scans were measured at 350 W, 93.9 eV constant pass energy, and 0.3 eV energy step. The binding energies were adjusted by setting the adventitious carbon signal to 284.8 eV. Surface concentrations are calculated by integrating the peaks areas and using standard atomic sensitivity factors supplied by the equipment manufacturer. In_2O_3 powder (99.997%, Puratronic, Alfa Aesar) and In foil (99.99%, Alfa Aesar) were measured as references.

XRD measurements were conducted on a Bruker D8 instrument equipped with Mo K_α radiation onto 2 cm^2 electrodes of ~3 μm starting thickness (equivalent weight around 4–5 mg). Electrodes were extracted from coin cells inside an Ar glovebox and pressed onto a fiber paper to remove the remaining electrolyte. With Na, some cells were short-circuited at room temperature or inside an oven at 65 °C for 40 h. Samples were sealed onto a glass slide with Kapton tape (25 μm), sealed inside an Ar-filled pouch bag and transported to the diffractometer, as performed earlier [2,4,7,12–15]. XRD scans were acquired for a total time of 80–100 min, typically from 5 to 35° 2θ (Mo K_α), with 0.03 or 0.04° step size and 6–8 s step time.

SEM micrographs were acquired using a JEOL JSM-6500F Field Emission SEM.

3. Results and discussion

3.1. Electrochemical reaction of indium with Li

The as-prepared films consist of relatively smooth grains covering the rough Cu substrate, softening the original Cu foil morphology (Fig. 1a). XRD reveals quasi phase purity, with a very small amount of copper indium (Fig. 1b). The presence of copper indium results from intermixing between Cu and In during the sputter deposition. Rietveld refinement of the XRD pattern gives lattice parameter values of $a = b = 3.247$ Å (±0.001) and $c = 4.939$ Å (±0.002) for tetragonal I4/mmm indium crystal structure. This result agrees closely with values $a = b = 3.251$ Å and $c = 4.945$ Å

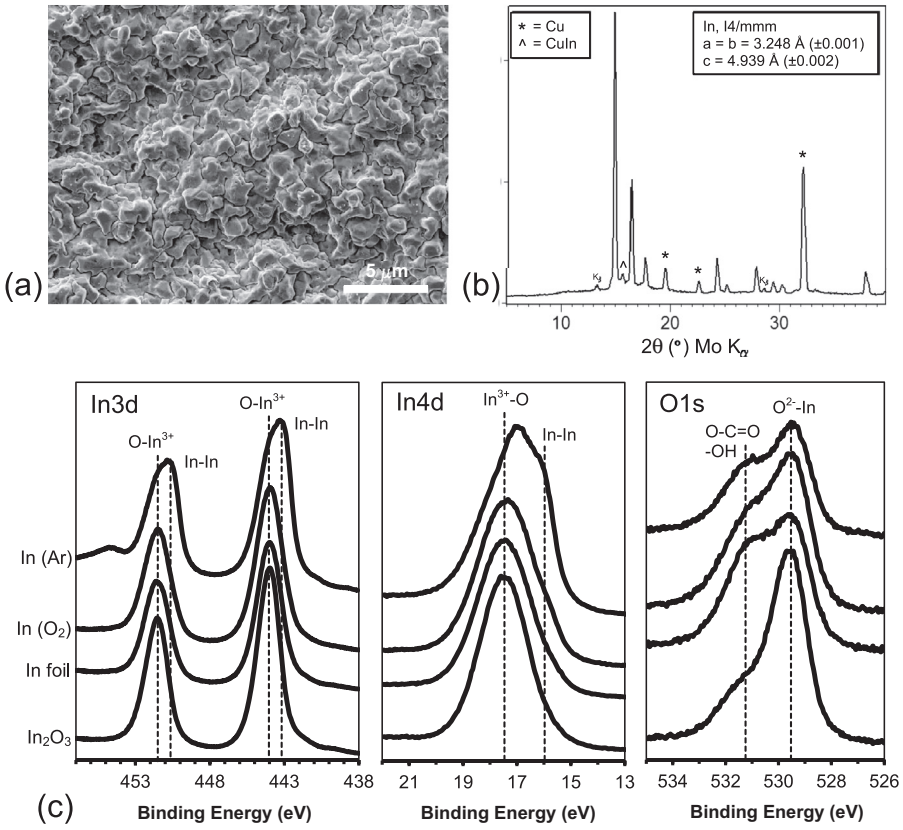

Fig. 1. Microstructural and surface properties of the starting films measured with SEM, XRD, and XPS. (a) Representative SEM photograph, (b) XRD pattern of films deposited onto roughed Cu foil, and (c) In3d, In4d, and O1s XPS core level spectra for pristine films stored in an argon glovebox, pristine films stored in a dry (O_2) box, a foil exposed to air for several months, and In_2O_3 powder.

from the PDF database (PDF 01-085-1409). Inspection of the films by XPS (Fig. 1c) shows that the pristine films, stored in a sealed bag within an Ar glovebox, are partially oxidized due to air exposure after preparation. This is visible from the In3d core level spectrum and is further supported by the In4d core level spectrum, as compared to a reference In_2O_3 powder. The bulk of the film, however, has a metallic character evidenced by a shoulder around 443.3 eV in In3d5/2, the presence of a In3d5/2 shake-up satellite around 455 eV characteristic of the metal (In3d3/2 shake-up satellite around 463 eV) as well as a shoulder near 16 eV in In4d. In contrast, an indium film stored in a dry air filled box containing O_2 has a larger amount of oxide formed on the surface and signals mostly corresponding to In_2O_3. Similarly, an In foil stored in air for several months is almost fully oxidized on the surface with only a very weak shoulder visible around 16 eV in the In4d spectrum to indicate the presence of metallic In. The results illustrate that the indium surface will readily oxidize to In_2O_3 when exposed to air even for a few minutes, which is significant because indium oxides appear to strongly affect the electrolyte decomposition (see later).

The electrochemical profile of cells containing Li with an EC/DMC electrolyte, cycled from 0 to 2 V, is dominated by a plateau at 1.4 V (Fig. 2a) during discharge. This plateau is a result of anomalous electrolyte decomposition, as observed for pure Sn during the reaction with Li [26] or with Na [2], and is not related to the conversion of In_2O_3 normally measured at 1.2 V [24]. This electrolyte decomposition is referred to as anomalous as it is outside the normal electrochemical window of decomposition typically considered below 1 V vs Li/Li^+. Moreover, the reaction consumes a large amount of charge and importantly limits the storage capacity of the electrode material (Fig. 2a). The anomalous reaction was proposed to result from the catalytic activity of the pure metal to importantly promote the decomposition of the electrolyte, which could eventually be suppressed by using lower charge voltage cut-off or higher currents [26]. This decomposition has been thought to result in the formation of a thick surface layer which eventually passivates the electrode surface and block Li transfer at the electrolyte interface [26]. We suspect that this pronounced reaction results in fact from the catalytic activity of the native surface oxides for a given salt/solvent electrolyte mixture. Although the side reaction was not observed for pure In_2O_3 films cycled in 1 M $LiClO_4$ in propylene carbonate (PC) [24], the absence of reaction is likely related to the use of perchlorated salts in PC, which do not seem to favor as much the anomalous electrolyte decomposition. This hypothesis is supported by the absence of an anomalous reaction between Sn thin films and 1 M $LiClO_4$ in PC [27] whereas the anomalous decomposition was readily observed in $LiPF_6$-based electrolyte [26].

One way to suppress the pronounced electrolyte reaction is to increase the discharge current significantly till the reaction at 0.6 V is reached (not presented). Another way consists of incorporating the FEC electrolyte additive (5 wt%) for samples stored in Ar, and restricting the charge voltage to 1.1 V prevent the anomalous electrolyte decomposition during the first and subsequent cycles (Fig. 2b). The corresponding potential profile exhibits a plateau at 0.6 V during discharge, corresponds to 1 Li/In, followed by two successive slopes from 1 to 1.5 Li/In centered at 0.25 V, and a large plateau from about 1.5 to 4.5 Li/In centered at 0.03 V (Fig. 2b). During charge, the profile is primarily characterized by three initial plateaus (0.09 V, 0.13 V and 0.25 V), two successive slopes (centered at 0.37 V), and a final plateau (0.6 V). A comparative analysis of the

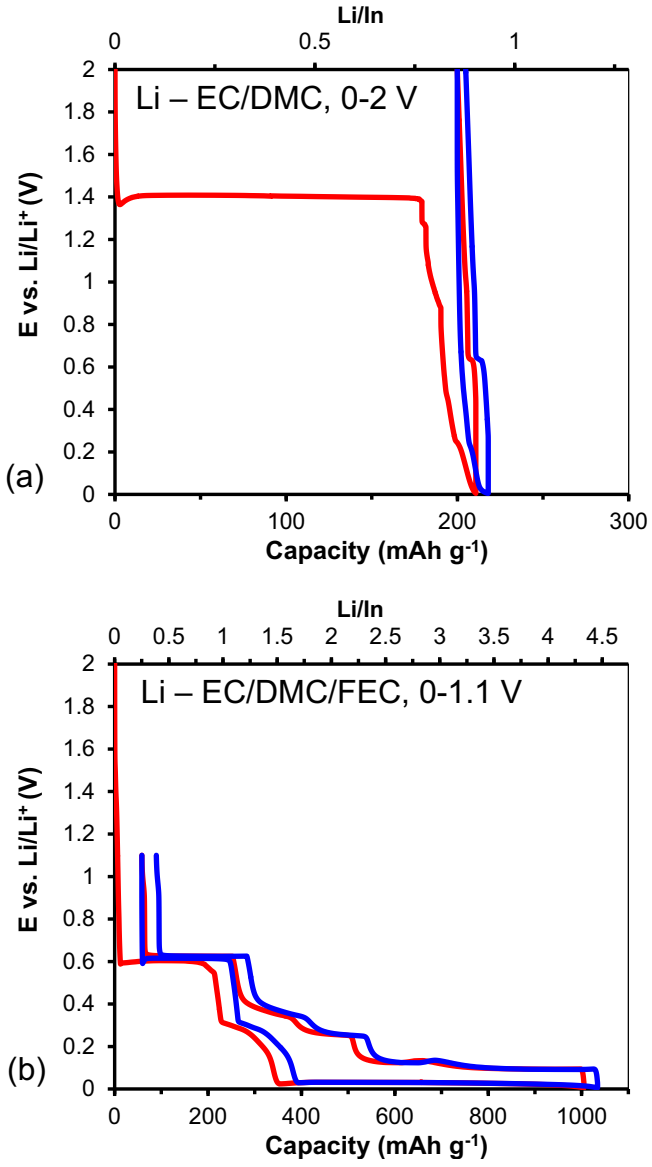

Fig. 2. Potential profiles of indium thin film electrodes for the reaction with Li at 50 μA cm^{-2} in (a) EC/DMC and (b) EC/DMC/FEC (5 wt%) electrolyte solutions. Red and blue curves are for the 1st and 2nd cycles respectively. (For interpretation of the references to colour in this figure legend, the reader is referred to the web version of this article.)

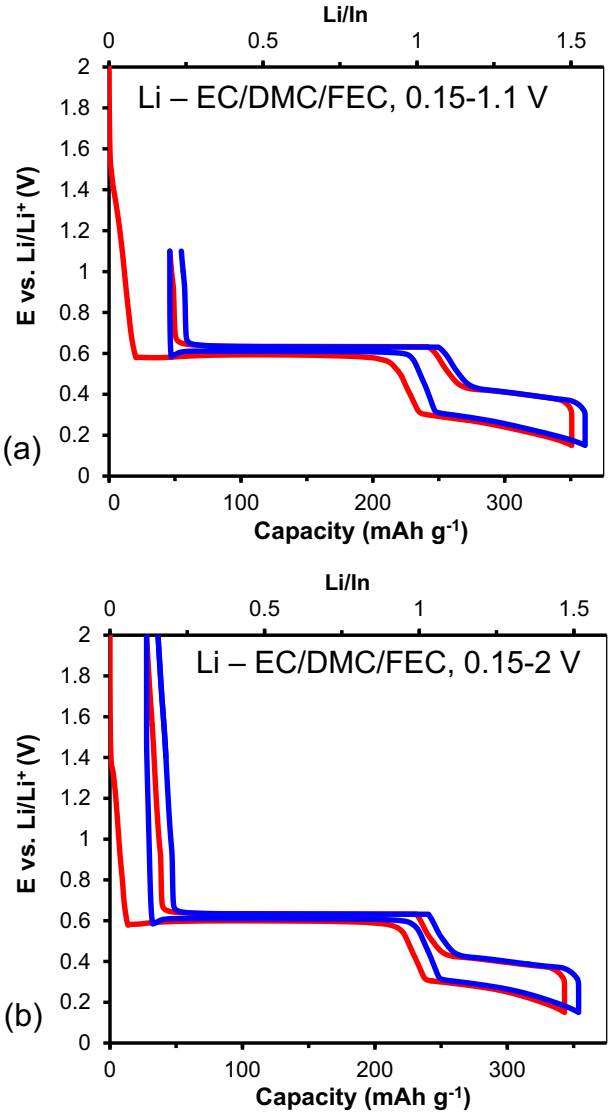

Fig. 3. Potential profiles of indium thin film electrodes for the reaction with Li in an EC/DMC/FEC(5 wt%) electrolyte solution at a current of 50 μA cm^{-2} from (a) 0.15–1.1 V and from (b) 0.15–2 V. Red and blue curves are for the 1st and 2nd cycles respectively. (For interpretation of the references to colour in this figure legend, the reader is referred to the web version of this article.)

profile over a range of 0.15–1.1 V (Fig. 3a) illustrates that the (dis) charge plateaus occurring at 0.6 V represent the same reaction. Similarly, the two reactions represented by the successive slopes centered at 0.25 V during discharge and the two slopes around 0.37 V during charges are conjugated. This implies that the third large plateau at 0.03 V of the discharge is related to the first three plateaus which appear at 0.09, 0.13 and 0.25 V during charge (Fig. 2b).

A series of experiments were performed to understand the role of FEC and extent of lithiation on the electrochemical properties of the electrodes. The data shows that the FEC additive significantly limits the electrolyte decomposition in the first and subsequent cycles over the range of 0–1.1 V (Fig. 2b), as well as over the range of 0.15–1.1 V (Fig. 3a). Extending the charge cut-off to 2 V for cycling from 0.15 to 2 V (Fig. 3b) does not induce the presence of a plateau around 1.4 V during the second cycle, which indicates that the anomalous electrolyte decomposition does not take place under these conditions. However, it is particularly interesting to note that the effectiveness of the FEC electrolyte additive in hindering the electrolyte decomposition is limited to the first discharge when the discharge cut-off voltage is extended to 0 V and the first charge is conducted up to 2 V (Fig. 4a). Indeed, the electrolyte decomposition represented by a plateau at 1.4 V occurs in the second cycle even in the presence of 5 wt% FEC additive (Fig. 4a).

This finding is rather surprising as the charged state from which the discharge begins is generally believed to dictate the anomalous electrolyte decomposition [26]; here, however, the reaction is influenced by the extent of the discharge preceding the charge at 2 V (Figs. 3b and 4a). In the case of Li–Sn electrodes, the anomalous electrolyte decomposition was proposed to result from the formation of metallic Sn on the surface, acting as catalyst when the charge is conducted at high values such as 2 V [26]. Restricting the charge cut-off was thought to result in the presence of Li_xSn, which would not catalytically decompose the electrolyte [26]. We have

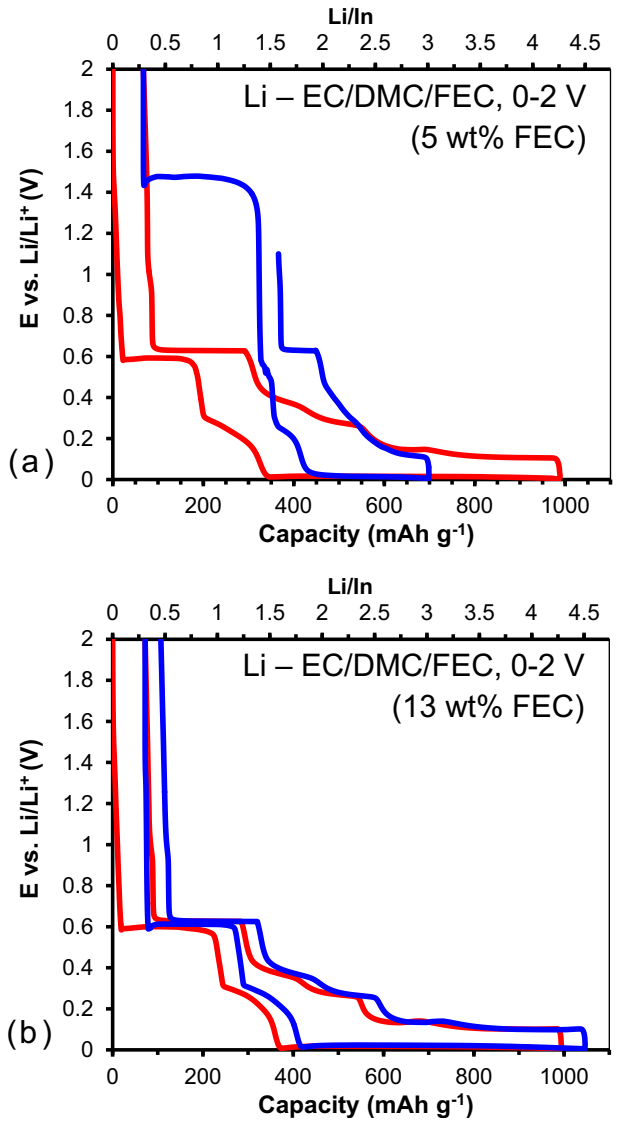

Fig. 4. Potential profiles of indium thin film electrodes for the reaction with Li in (a) 5 wt% FEC and (b) 13 wt% FEC electrolyte solutions at a current of 50 μA cm^{-2} from 0 to 2 V. Red and blue curves are for the 1st and 2nd cycles respectively. (For interpretation of the references to colour in this figure legend, the reader is referred to the web version of this article.)

shown recently for Sn cycled with Na that the catalytic decomposition of the electrolyte is in fact related to oxidized Sn species and not metallic Sn [2]. Similarly here, as the surface of air-exposed indium is always covered by an oxide (Fig. 1c), it is not surprising to measure the electrolyte decomposition in the absence of FEC. Moreover, it is interesting to observe that the presence of 5 wt% FEC does not always guarantee the suppression of the anomalous electrolyte decomposition during the second discharge. In addition, we observed that the presence of 5 wt% FEC does not fully suppress electrolyte decomposition during the first discharge if the surface is highly oxidized. Films stored in a dry air purge box (O_2 present) have a surface composition of $InO_{1.60}$ including the O related to C surface species and hydroxides, or $InO_{0.90}$ excluding these other O species. Interestingly, we found that these samples, which have a thicker surface oxide layer compared to samples stored in Ar (Fig. 1c), as well as samples prepared at a base pressure of 2×10^{-6} Torr or more, which promotes O contamination, systematically exhibited the anomalous electrolyte reaction when 5 wt% FEC is used (not presented). In contrast, films stored under Ar have a surface composition of $InO_{0.95}$ including the O related to C surface species and hydroxides, or $InO_{0.48}$ excluding these O species, and do not provoke the anomalous electrolyte decomposition during the first discharge when 5 wt% FEC is used (Fig. 2b). These results support the hypothesis that the presence of a larger amount of oxides favors the catalytic electrolyte decomposition even in the presence of 5 wt% FEC.

It is intriguing that for a charge cut-off of 2 V the presence of 5 wt% FEC only prevents the anomalous electrolyte decomposition when the discharge cut-off is limited to 0.15 V (Figs. 3b and 4a). When the discharge is limited to 0.15 V, the amount of unreacted FEC may be larger compared to an electrode discharged to 0 V. In turn, the larger amount of FEC can provide protection during the following cycles when discharges are restricted to 0.15 V. An electrolyte with a higher amount of FEC, i.e. 13 wt% (Fig. 4b), was applied to determine if the presence of decomposition during the second discharge may be related to the insufficient concentration of FEC. During the cycling from 0 to 2 V, the electrochemical profiles measured during several cycles, of which the first two are reported in Fig. 4b, confirm that the larger amount of FEC provides suitable protection during cycling from 0 to 2 V. Hence, we suppose that with a lower concentration (5 wt%), the majority of FEC may have been consumed during the first discharge to 0 V and that the passivation products of FEC may have been partially removed from the surface and cannot be effectively replaced. After an electrochemical cycle, the increased surface area (rougher surface) (Fig. 5)

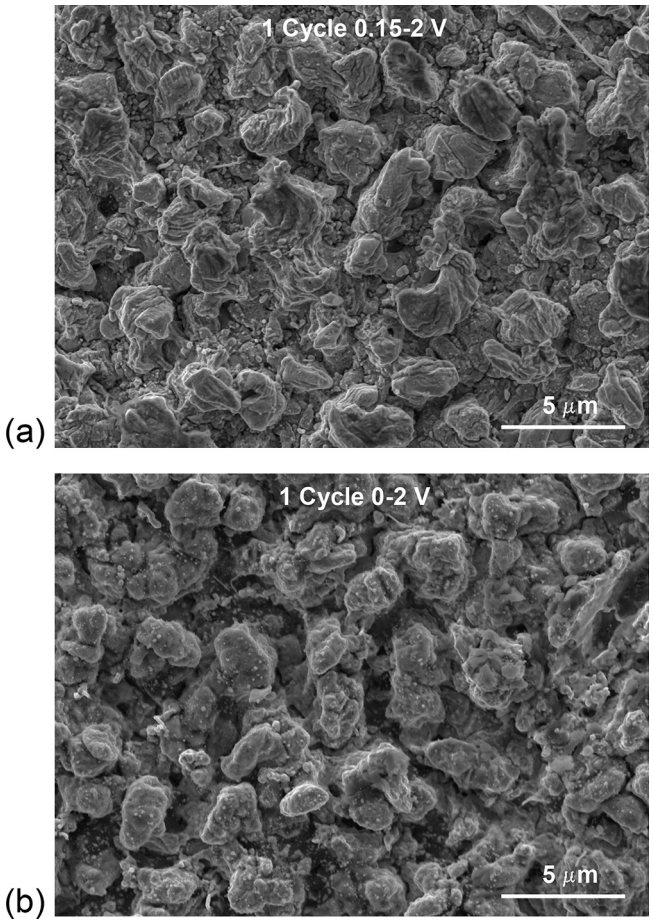

Fig. 5. Surface morphology of cycled indium thin film (~0.8 μm) electrodes measured with SEM. Representative SEM photographs of charged electrodes (2 V) after 1 cycle with Li from (a) 0.15–2 V and (b) 0–2 V.

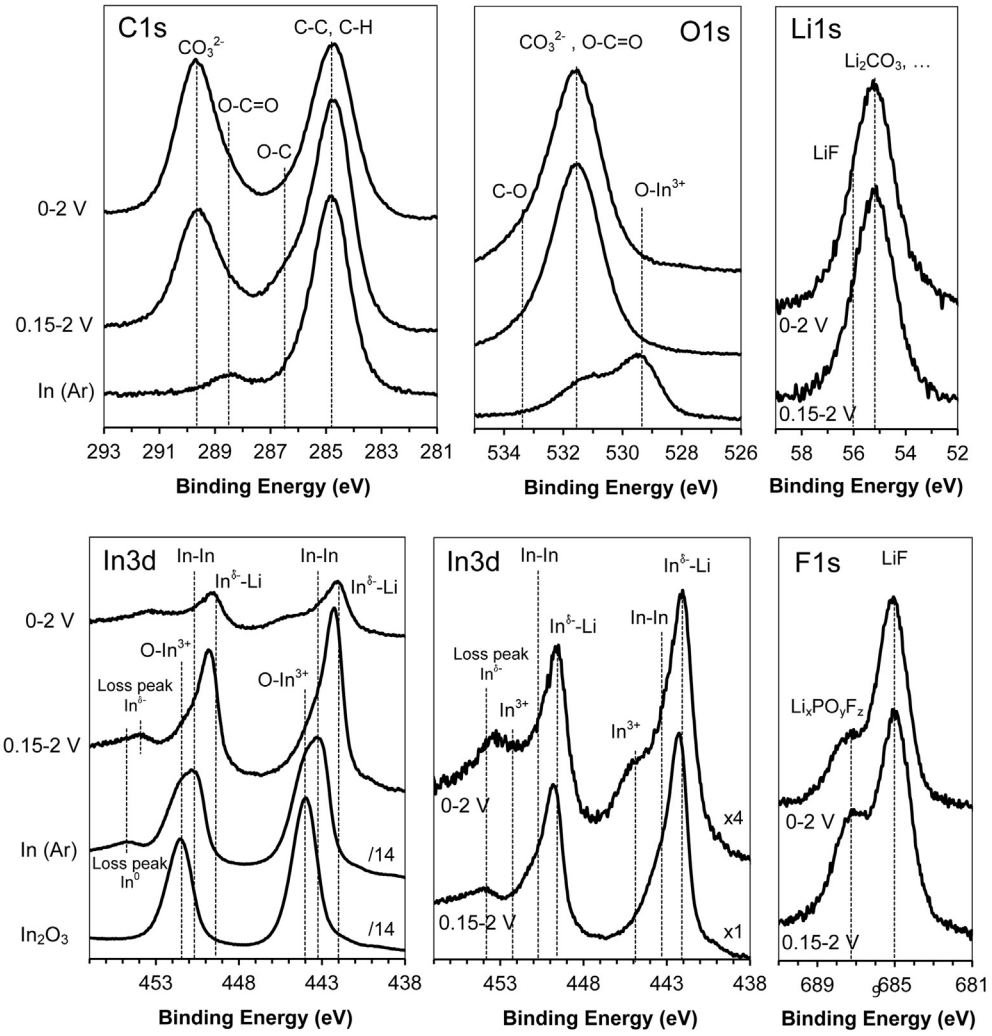

Fig. 6. Surface chemistry of charged electrodes (2 V) after 1 cycle with Li from 0.15 to 2 V and 0–2 V. C1s, O1s, F1s and Li1s XPS high resolution core level spectra for pristine and cycled electrodes (bottom to top). In3d core level spectra are for In_2O_3 powder, pristine film, and cycled film electrodes (bottom to top).

may also promote the consumption of FEC as well as favor the electrolyte reaction.

The reasons for the decomposition of the electrolyte during the second discharge when using 5 wt% FEC have been further explored by studying the surface morphology using SEM and the surface chemistry using XPS for charged electrodes (2 V, Li free) pre-discharged with different cut-off voltages, i.e. 0 and 0.15 V. The SEM images taken for each electrode after one cycle are shown in Fig. 5. Discharging to 0.15 V is equivalent to the reaction of approximately 1.5 Li/In, versus 4.33 Li/In when the discharge is conducted down to 0 V (see XRD), corresponding to predicted expansions of 83% and 297%, assuming the formation of Li_3In_2 (PDF 01-071-1338) and $Li_{13}In_3$ (PDF 03-065-7421) from In (PDF 01-085-1409), respectively. For both electrodes, large domains of several microns are visible along with smaller particles. The increased roughness of the cycled electrodes over that of the pristine material is a result of the volume changes to which the electrodes were subjected. The texture of the electrode cycled from 0.15 to 2 V bears a closer resemblance to that of the pristine material (Fig. 1a), evidenced by the presence of smoother features. Restricting the discharge at 0.15 V significantly lessens the volume change and therefore does not alter the large domains as much as when the voltage range is extended to 0 V, during which the reaction proceeds to its full extent. It is clear that the surface area increases significantly compared to the pristine material, possibly supporting further that a sufficient amount of FEC is essential to protect the surface effectively. However, it is not obvious that the difference in surface area or particle morphology, based on the size and shape of the domains, is significant enough to explain the difference in electrolyte decomposition between the discharges at 0.15 and 0 V.

The surface chemistry of these charged electrodes (2 V) has been studied by XPS (Fig. 6) to unravel the possible origins of the electrolyte decomposition when cycling with FEC from 0 to 2 V. Analysis of the XPS results for the In3d core level spectra shows a significant difference in the intensity of the signals, with less indium measured on the surface for the electrode cycled from 0 to 2 V. Concomitantly, the solid electrolyte interphase (SEI) products (carbonates, carboxylates/esters, ethers) are in somewhat larger quantity, as visible from the C1s and O1s signals. The presence of a larger amount of electrolyte products likely results from the application of the more negative (reducing) discharge potential of 0 V. Moreover, in both cases the presence of LiF and $Li_xPO_yF_z$ species is evidenced by the Li1s and F1s signals. LiF can result from the decomposition of $LiPF_6$ or FEC, whereas $Li_xPO_yF_z$ comes from the reaction of $LiPF_6$. Interestingly, the indium spectra show small but significant differences. In the case of the electrode cycled from 0.15

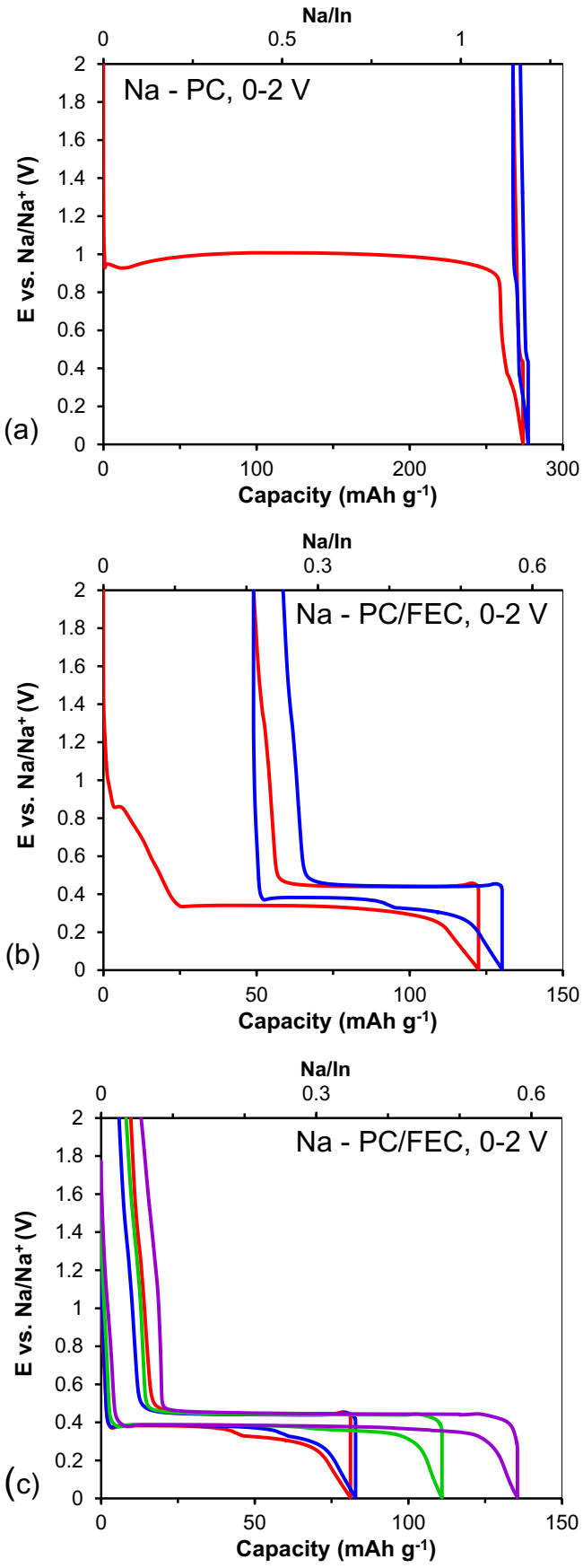

Fig. 7. Potential profiles of indium thin film electrodes for the reaction with Na at 10 μA cm^{-2} in (a) PC (b) PC/FEC (5 wt%) electrolyte solutions. Red and blue curves are for the 1st and 2nd cycles respectively. (c) shows the evolution of selected potential profiles: red, blue, green and purple curves are for the 2nd, 5th, 10th, and 15th cycles, respectively. (For interpretation of the references to colour in this figure legend, the reader is referred to the web version of this article.)

to 2 V, indium has mostly a reduced ($In^{\delta-}$—Li) character, as supported by the In3d binding energy around 442 eV lower than that expected for the metal (443.3 eV), as well as the presence of the In3d5/2 shake-up satellite now around 454 eV. Additionally, the electrode shows a small proportion of metallic In—In, as characterized by a shoulder around 443.3 eV in In3d5/2. The electrode cycled from 0 to 2 V also presents features for reduced $In^{\delta-}$—Li and metallic In—In species. However, it displays signals at unusually high binding energies as well, around 445 eV for In3d5/2 and 452.5 eV for In3d3/2. These signals arise from an oxidized In^{3+} species which may be responsible for the catalytic decomposition of the electrolyte when cycling from 0 to 2 V. The environment of these In^{3+} species cannot be O^{2-} only, and may be related to OH^- or F^- ligands, evidenced at binding energies of 445 eV or higher [28,29]. The formation of oxidized species is similar to what was measured for Na—Sn electrodes, which, after a full charge at 2 V, showed the presence of Sn^{4+} species responsible for the anomalous electrolyte decomposition [2]. Aging at 2 V for 17 h allowed the oxidized surface species to relax to lower oxidation states, and the electrolyte decomposition was concomitantly suppressed [2]. Although these oxidized species can explain here the origin of the electrolyte decomposition, it is not clear why these species would be present only when discharging to 0 V.

3.2. Electrochemical reaction of indium with Na

The electrochemical profile of cells containing Na with a PC-based electrolyte, cycled from 0 to 2 V, is dominated by a plateau at 0.9 V (Fig. 7a) during discharge, due to electrolyte decomposition [2,26]. As measured with Li, incorporating the FEC additive notably limits this reaction. A small plateau at 0.9 V is still visible during the first discharge, but it does not detrimentally affect the rest of the profile. In addition, cycling from 0 to 2 V does not result in the presence of an anomalous plateau around 0.9 V during the subsequent cycles even with a discharge cut-off of 0 V. This difference with Li is likely related to the large difference in volume expansion due to the concentration of inserted Li and Na. Assuming the formation of $Li_{13}In_3$ (see XRD results), the volume expansion with Li amounts to 297%. In contrast, since the reaction with Na is limited to 70–125 mAh g^{-1} depending in the cycle number (Fig. 7b and c), a much lower volume expansion is expected (37–65%, assuming a linear relationship between the amount of Na and the electrode volume). Due to this lower volume change, the SEI passivation layer may be able to mechanically cope with the much lower volume expansion/shrinkage such that the electrode surface is not exposed at full charge when cycling with Na. In addition, the amount of remaining FEC may be much larger as the storage capacity with Na is much lower and the discharge potential profile is significantly more positive than with Li. Therefore, FEC additive could effectively passivate the surface upon long cycling even when the charging is conducted up to 2 V.

For the first cycle with Na, the potential profile is characterized during discharge by the small plateau at 0.9 V as well as a larger plateau at 0.34 V; upon charging, there is a single plateau around 0.44 V (Fig. 7b). Interestingly, during the second discharge, the profile is characterized by two plateaus, one at 0.38 V and the other at 0.31 V (Fig. 7b). Upon cycling, the distinction between the two plateaus at 0.38 V and 0.31 V becomes less pronounced until the fifteenth cycle where they

appear seamless (Fig. 7c). As will be discussed later with XRD results, the reaction of indium with Na is severely limited such that indium persists in short circuited cells placed in an oven at 65 °C. This suggests that the diffusion of Na into the bulk is severely limited. Another interesting feature which arises upon cycling is the increase in capacity. The capacity increases from about 75 mAh g^{-1} in the second cycle to 125 mAh g^{-1} in the fifteenth cycle (Fig. 7c). While the increase in capacity is significant, the most reversible capacity achieved remains far below the theoretical capacity of 467 mAh g^{-1} for the In–Na system assuming the formation of Na_2In [18]. In comparison, a reversible capacity of 950 mAh g^{-1} is achieved by the Li cells cycled from 0 to 1.1 V, which match closely the theoretical value of 1012 mAh g^{-1} assuming the formation of $Li_{13}In_3$ [17]. The increase in Na capacity is possibly related to an improvement of the reaction kinetics due to the formation of smaller particles with a large surface area, such that Na can penetrate deeper inside the bulk of the film or of indium particles upon repeated cycling. In addition, an improvement of the reaction kinetics could explain why the potential of the second plateau increases (Fig. 7c).

3.3. Comparison of overpotentials during charging and discharging

The potential profiles measured using a low constant current and quasi-equilibrium GITT are compared in Fig. 8a and b for Li and Na, respectively. The CC vs. GITT results show relatively low overpotentials for both Li and Na, particularly while charging. However, an increase in overpotential is clearly visible above 1 Li/In, particularly from 1 to 1.75 Li/In, which may indicate a kinetic limitation for diffusion during the cation insertion reaction. Interestingly, this composition range corresponds to the formation of unknown crystal structures (see XRD). For Na, the larger overpotentials are dominant at capacities over 40 mAh g^{-1} when the second plateau appears (Fig. 8b). The relatively small overpotentials during cation removal highlight the good prospects of indium for high rate applications (see later).

3.4. XRD characterization of reaction products

The reaction mechanism of the electrode was investigated during discharge/charge for both ion systems for the electrochemical positions presented in Fig. 9. The corresponding XRD patterns obtained with Mo K_α radiation are presented in Fig. 10 for Li and Fig. 11 for Na. Mo K_α radiation was chosen for these tests as it is much more penetrating than Cu K_α and enables a better determination of the material structure when using Kapton to protect the samples during *ex situ* measurements [2]. The reaction of In with Li at high temperatures can lead to the formation of various phases with widely varying crystal structures: $Li_{0.3}In_{1.7}$, LiIn, Li_5In_4, Li_3In_2, Li_2In and $Li_{13}In_3$ ([17], PDF database), and several others such as tentatively Li_7In_4, $LiIn_3$ and Li_7In, for which no crystallographic data is available [17]. During the electrochemical reaction with Li (Fig. 10), the material formed during lithiation at 0.7 V is nearly identical to the pristine film with very similar lattice parameters (Table S1). At this position, there is evidence for the disappearance of copper indium into, likely, Cu and Li_xIn. After the plateau at 0.6 V, indium reacts to a large extent to form LiIn, as visible on the patterns collected at 0.55 V and 0.32 V. In both cases a small amount of indium remains, with the amount of indium being less in the latter case, as expected. Further lithiation leads to the formation of unknown phases at 0.25 and 0.15 V [17] accompanied with the disappearance of LiIn. These potentials are within the range of composition where the formation of Li_5In_4 could be expected (Fig. 9a), though not evidenced, and where the increase in overpotentials in the most substantial (Fig. 8a). The large overpotentials

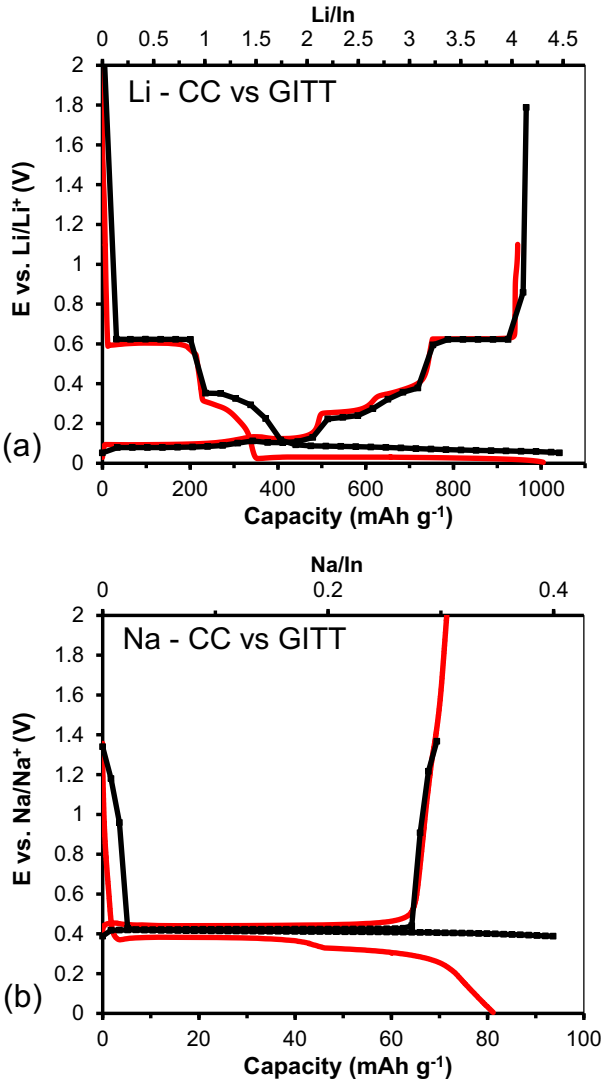

Fig. 8. GITT potential profiles (connected markers) during the reaction with (a) Li and (b) Na. The constant current profiles obtained during the first cycle are included as reference (red). (For interpretation of the references to colour in this figure legend, the reader is referred to the web version of this article.)

would indicate significant kinetic sluggishness possibly due to the formation of crystal structures with higher energy barriers for diffusion. During further discharge on the large plateau at 0.03 V, the formation of Li_2In and $Li_{13}In_3$ phases are evidenced (Fig. 10, Table S1).

We discussed earlier that the plateau at 0.03 V obtained during discharge is conjugated with three plateaus at 0.09, 0.12 and 0.25 V during charge. We observe that during Li-ion removal the reaction proceeds by the conversion of $Li_{13}In_3$ into Li_2In in two stages along the plateaus at 0.09 and 0.12 V. The intermediate position coincides with the electrochemical composition of Li_3In but no crystallographic data is available for such a phase. The origins of the two plateaus is not known but may be related to the removal of Li from different crystallographic sites within $Li_{13}In_3$, ultimately leading to the formation of Li_2In. Further delithiation on the plateau at 0.25 V leads to the formation of Li_3In_2. The rest of the charge is characterized by the formation of LiIn followed by that of indium, and ultimately copper indium, which was initially present as an impurity. These results demonstrate the exceptional reversibility of the reaction. As

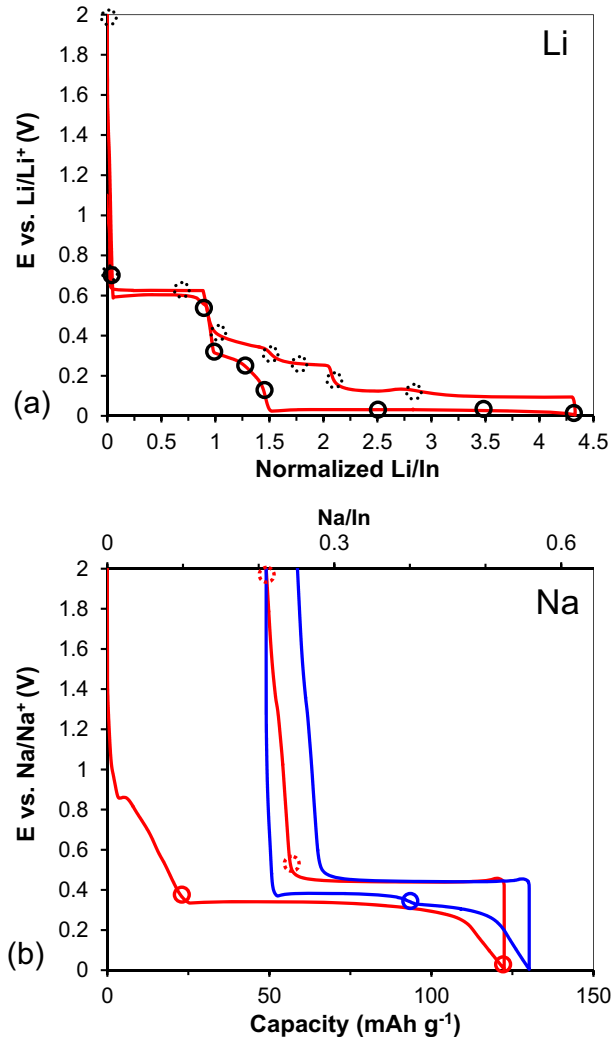

Fig. 9. Selected positions on the electrochemical curves for XRD characterization (see Figs. 10 and 11). Full and dashed markers correspond to positions during discharge and charge, respectively.

during discharge, the presence of Li_5In_4 was not evidenced, however, the formation of Li_3In_2 was clearly revealed during charge. We suspect that this phase can form during discharge but we did not capture this specific position during our *ex situ* experiment. In summary, all Li–In phases with known crystal structures, with the exception of Li_5In_4, have been evidenced to form during the electrochemical reaction with Li.

The reaction of indium with Na at high temperatures can lead to the formation of various compounds: $Na_{15}In_{27.4}$, $Na_7In_{11.6}$, NaIn and Na_2In [18]. For electrodes cycled with Na (Fig. 9b), the patterns of the electrode discharged at 0.36 V during the first cycle (0.36 V #1) before the plateau occurs shows the diffraction lines of pure indium (Fig. 11). After discharging to 0 V the pattern displays strong features of indium with one weak peak related to an unknown crystal structure. A short-circuited cell placed in an oven at 65 °C was also characterized. For this cell, the pattern dominantly shows the diffraction lines of indium along with weak peaks for NaIn, and peaks related to the unknown phase. Upon charging at 0.5 or 2 V, the patterns consist of the reflections of pure indium. During the second discharge, the pattern collected at 0.36 V (0.36 V#2, in between the two plateaus, *c.f.* Fig. 9b) shows the diffraction peaks of indium and weak peaks corresponding to an unknown phase. The weak peaks corresponding to the unknown phase form in the same positions over the first two cycles and do not match the patterns of $Na_7In_{11.6}$ or $Na_{15}In_{27.4}$. In addition, no evidence for the formation of NaIn or Na_2In is found at room temperature. The absence of formation of $Na_7In_{11.6}$ or $Na_{15}In_{27.4}$ may be related to the complexity of these Zintl phase structures [18]. At 65 °C, however, it is clear that NaIn can partly form. Overall, the results support that the electrochemical reaction of indium with Na is importantly limited.

Since we observe that the extent of the reaction with Na progresses upon cycling at the same electrochemical potential (Fig. 7c), we do not think that the thermodynamics of the reaction limits the initial insertion of Na ions. Moreover, as the persistence of indium is measured for cells short-circuited at 65 °C for 40 h, we suspect that the reaction is hindered by very slow diffusion kinetics of Na. The phase responsible for the slow diffusion of Na could be the unknown Na_xIn phase that forms on the surface of indium. Analogously, Cu_6Sn_5 readily reacts to the full extent with Li but has a very limited reaction with Na due to the larger size of Na compared to Li [12].

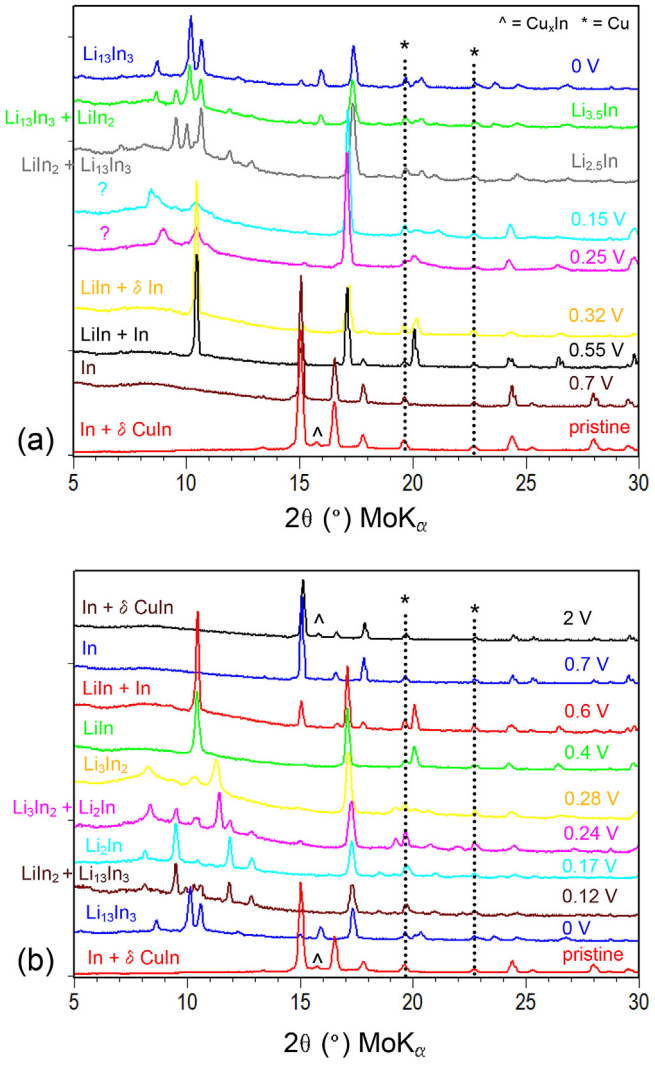

Fig. 10. XRD patterns obtained during (a) discharge and (b) charge for indium thin film electrodes during the reaction with Li at the various positions given in Fig. 9. The labels on the right handside indicate the electrochemical positions whereas the labels on the left handside correspond to the identified phases. Refinements of the corresponding lattice parameters are given in Table S1. (^) and (*) correspond to CuIn and Cu diffraction lines.

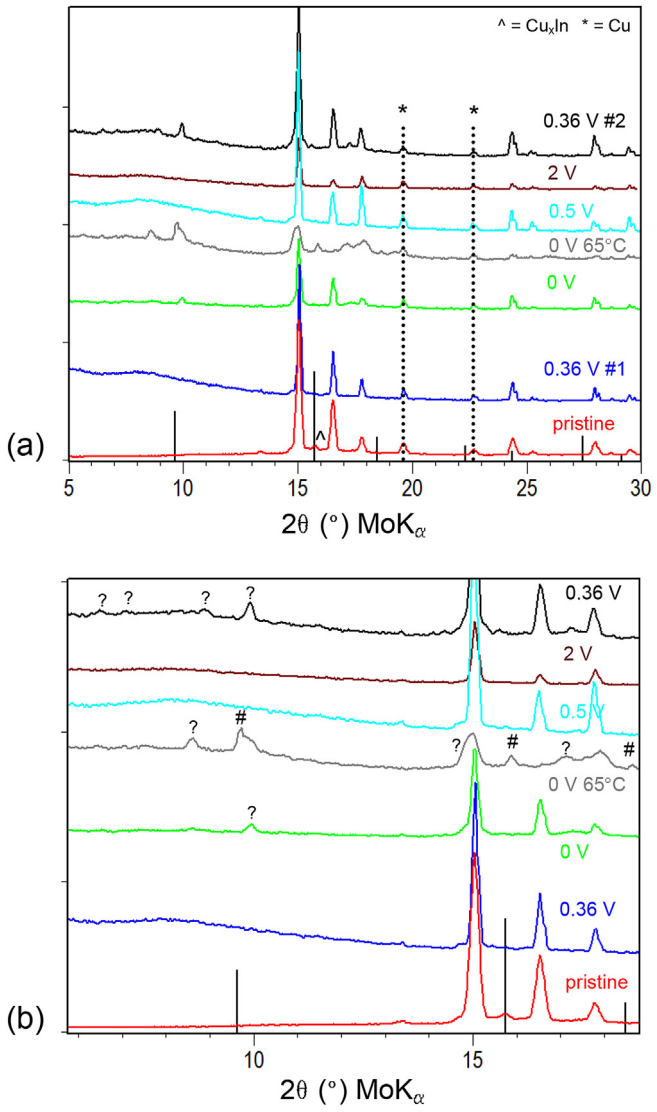

Fig. 11. XRD patterns obtained during discharge and charge for indium thin film electrodes during the reaction with Na at the various positions given in Fig. 9. (a) shows the full scale and (b) is a magnification of the low angles region. The labels on the right handside indicate the electrochemical positions. (^) and (*) correspond to CuIn and Cu diffraction lines. Vertical black bars are for NaIn reference pattern.

Although it apparently severely limits Na diffusion, we tested further whether the Na_xIn phase may allow Li diffusion. For that purpose, an electrode was short-circuited with Na for 60 h, recovered and rinsed with Li electrolyte. The cell was then assembled with Li in a FEC-based electrolyte. A stable open circuit voltage of 0.79 V vs Li/Li^+ was measured, which is equivalent to 0.46 V vs Na/Na^+ assuming 0.33 V voltage difference between Li/Li^+ and Na/Na^+. This value is fairly close to the measured equilibrium potential of 0.42 V (Fig. 8b) and supports that Na is present inside indium. The voltage profile of this electrode during the first cycle with Li shows features not only attributed to the reaction of indium with Li but also new features related to the reaction of Na_xIn with Li (Fig. 12). For instance, a discharge plateau is now evidenced at 0.23 V and several new charge features such as a plateau at 0.37 V, a slope around 0.55 V and a plateau near 0.8 V are measured (Fig. 12). In contrast, the profile during the second cycle is very close to what is obtained for pure In cycled with Li (Fig. 2b). The discharge plateau at 0.23 V likely represents the insertion of Li in the Na_xIn phase. During charge, the new charge features are thought to represent the removal of both Li and Na ions. This claim is supported by the larger charge capacity (ion removal) compared to the discharge (ion insertion) measured during the first cycle whereas pure indium normally shows of a larger discharge capacity (Fig. 2b) due to losses related to the SEI formation. In addition, the voltage profile during the second cycle is very similar to that of pure indium during the reaction with Li (Figs. 2b and 4b), which suggests that the charged electrode is made of pure indium. Hence, these findings support that the Na_xIn phase formed on the surface of indium allows Li diffusion, and other experiments (Figs. 7 and 11) indicate that the Na_xIn phase strongly hinders Na diffusion. Moreover, the results suggest the formation of ternary Li–Na–In phases, as indicated by the new (dis)charge features. Further work is required to explain the structural origins of the limited reaction with Na. In addition, theoretical works similar to that conducted on Na–Si by Malyi et al. [10,11] could provide useful insights on the origins of the limited reaction. Finally, the exploration of the Li–Na–In ternary diagram could yield the discovery of exciting new structures.

3.5. Electrode performance

The cycle life of the indium thin film electrodes is presented in Fig. 13a. When cycling with Li from 0 to 1.1 V, the initial capacity of about 950 mAh g^{-1} is followed by a sharp decline to around 100 mAh g^{-1} after 15 cycles. For the cycling performed with Li from 0.15 to 1.1 V or 2 V, the initial capacity is much lower at around 300–350 mAh g^{-1}, but the capacity is relatively stable for about 15 cycles. The following capacity fade, after 20 cycles, is pronounced with little capacity left after 30 cycles. When cycling is performed with Li from 0 to 0.5 V, the initial capacity of about 770 mAh g^{-1} is retained for about 15 cycles after which it gradually fades to about 400 mAh g^{-1} after 43 cycles (out of plot range). The improved capacity retention when cycling from 0 to 0.5 V cannot be explained by a significantly smaller volume expansion as this voltage range is responsible for the exchange of 3.33 Li/In, as the range 0–1.1 V accounts for 4.33 Li/In and the range 0.15–1.1 or 2 V corresponds to 1.5 Li/In (see XRD data). Two potential explanations are that preventing the formation of LiIn by limiting the charge at 0.5 V avoids the repeated transformation of cubic Fd-3m LiIn into tetragonal I4/mmm In, which may be mechanically detrimental. It could also be that the repeated electrolyte reduction/oxidation reactions are not as pronounced if charging is restricted to 0.5 V. Indeed, it is known that the SEI can reversibly partly oxidize, as shown on other Li and Na-based thin film electrodes at higher potentials [2,4,14,15]. Restricting at 0.5 V could thereby improve the stability of the electrode/electrolyte interface.

During galvanostatic cycling with Na from 0 to 2 V (Fig. 13a), the initial capacity slowly increases from about 70 mAh g^{-1} to 125 mAh g^{-1} over 20 cycles, but then experiences a sharp decline over the following cycles. When CCCV cycling is performed from 0 to 2 V (10/1 μA cm^{-2}) on a thinner electrode (0.2 μm) to try to maximize the reaction extent, the initial capacity of 120 mAh g^{-1} is held for 10 cycles after which it fades to about 30 mAh g^{-1} over the next 20 cycles. The application of CCCV with a cut-off current of 1 μA cm^{-2} allows for a much longer reaction time, and the use of a thinner electrode results in much shorter diffusion distances. These conditions suppress the capacity increase found when measuring with constant currents, thereby confirming the reaction hindrance due to limited kinetics, particularly diffusion, during the reaction with Na. Nevertheless, the application of CCCV is not sufficient to provide a capacity closer to the theoretical value.

The rate performance of ion removal from fully discharged (lithiated or sodiated) In thin film electrodes is presented in Fig. 13b for Li and in Fig. 13c for Na. The reaction kinetics of Li-ion removal

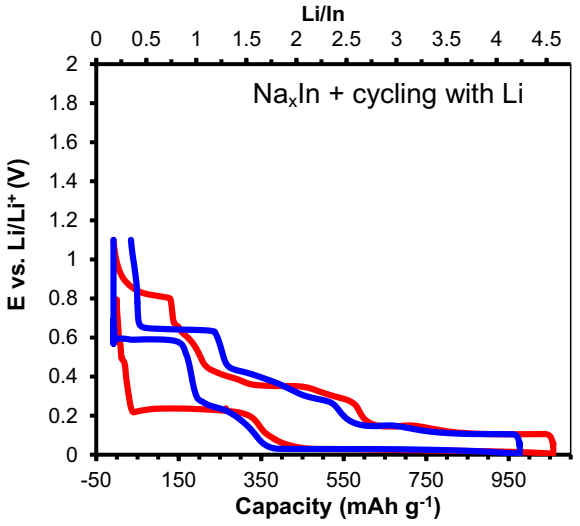

Fig. 12. Potential profiles of an indium thin film electrode (0.6 μm) short-circuited for 60 h with Na, recovered from the coin cell and rinsed with Li electrolyte, and measured with Li at 30 μA cm^{-2} in the EC/DMC/FEC (5 wt%) electrolyte solution. First and second cycles are shown in red and blue, respectively. (For interpretation of the references to colour in this figure legend, the reader is referred to the web version of this article.)

are very high, with nearly 100% of the maximum capacity retrieved at 10 C and more than 75% recovered at 100 C, corresponding to a charge in less than 30 s. The plateau present at 0.6 V for low currents is expected near the limit of 1 V set during the measurement at 100 C and it is reasonable to expect that 100% of the capacity could be retrieved at this high current if the charge cut-off would be extended up to 1.5 V. The increase in overpotentials is around 0.03 V at 0.1 C, 0.1 V at 10 C, and 0.5 V at 100 C (Fig. 9b). The reaction kinetics of Na-ion removal are quite good, with about 80% of the maximum capacity retained at 30 C. The increase in overpotentials is around 0.02 V at 0.1 C, 0.1 V at 10 C, and 0.2 V at 30 C (Fig. 13c). However, there is a remarkable increase and decrease of potential at the very beginning of the discharge, similarly to what is measured on pure Sb [4] and possibly attributed to limited nucleation/growth processes hindered by Na solid-state diffusion. The application of larger currents such as 100 C was therefore limited as the cut-off of 1 V was immediately reached. In order to verify that the rate performance is not influenced by the decrease in capacity retention from cycling, the potential profiles measured at the lowest current (0.1 C) following the rate test can be compared with the initial potential profiles performed at the same current value. For Li, the two profiles line up very well, confirming that the influence of cycling on the rate performance is negligible (Fig. 13b). Similarly for Na the voltage of the plateau voltage is the same, however, there is an increase in capacity for the profile obtained after the rate test (Fig. 13c). As discussed earlier, electrodes tested with Na experience an increase in capacity with cycling.

The electrodes cycled with Li over the voltage ranges 0.15 to 1.1 V (28 cycles), 0.15–2 V (29 cycles), 0–0.05 V (43 cycles), and 0–1.1 V (26 cycles) from Fig. 13a have been further studied by characterizing their surface morphology using SEM (Fig. 14). For the electrodes cycled from 0.15 to 1.1 V and 0.15–2 V, the surface of the film appears to be populated almost exclusively by small particles (Fig. 14a and b). The electrode cycled from 0 to 0.5 V shows what appear to be the beginnings of similar granulation but also larger domains and smooth features reminiscent of the starting material (Fig. 14c). This appearance could be a result of the fact that the electrode material cycled from 0 to 0.5 V and charged to 1.1 V did not undergo a "grinding" process induced by

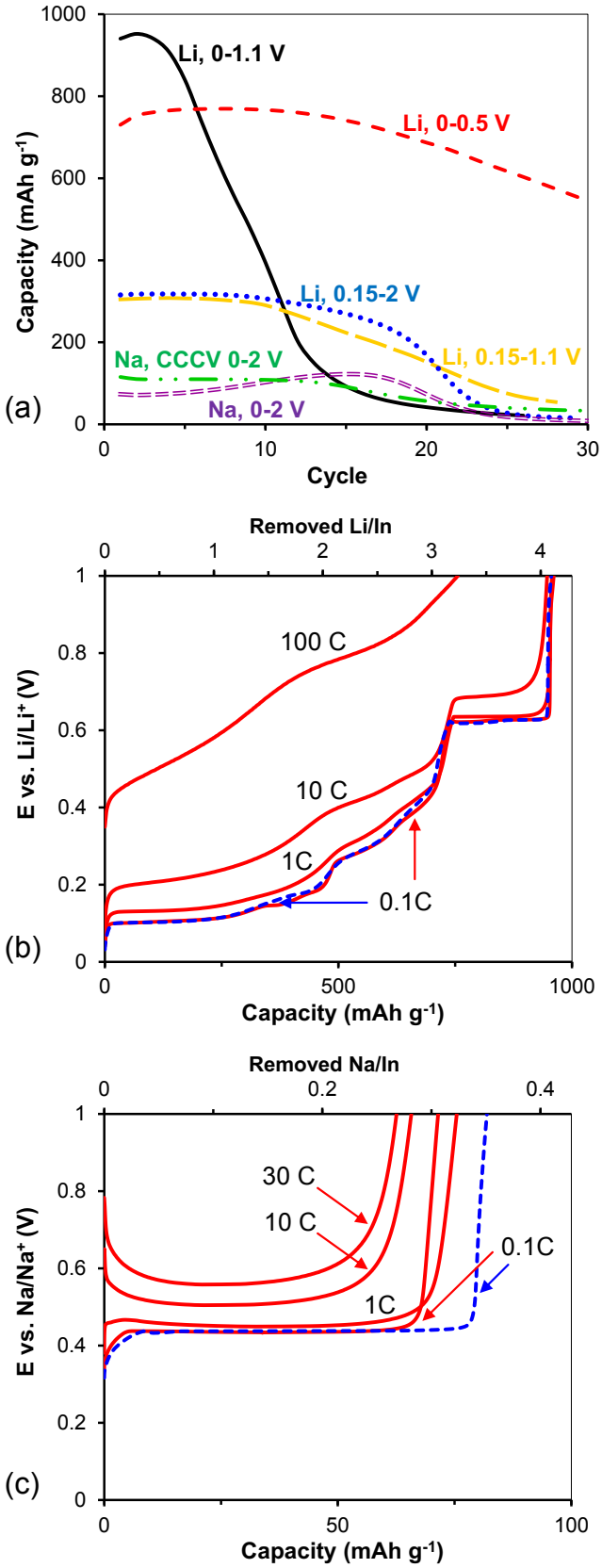

Fig. 13. (a) Capacity retention of indium thin film electrodes during the reaction with Li and Na, for various cut-off voltages. For the cycling with Li, films of ~0.8 μm were selected. For cycling with Na, the electrode galvanostatically cycled (CC) was 1.3 μm whereas the electrode subjected to CCCV was 0.2 μm. Rate performance of indium thin film electrodes during the reaction with (b) Li (0.6 μm) and (c) Na (0.5 μm).

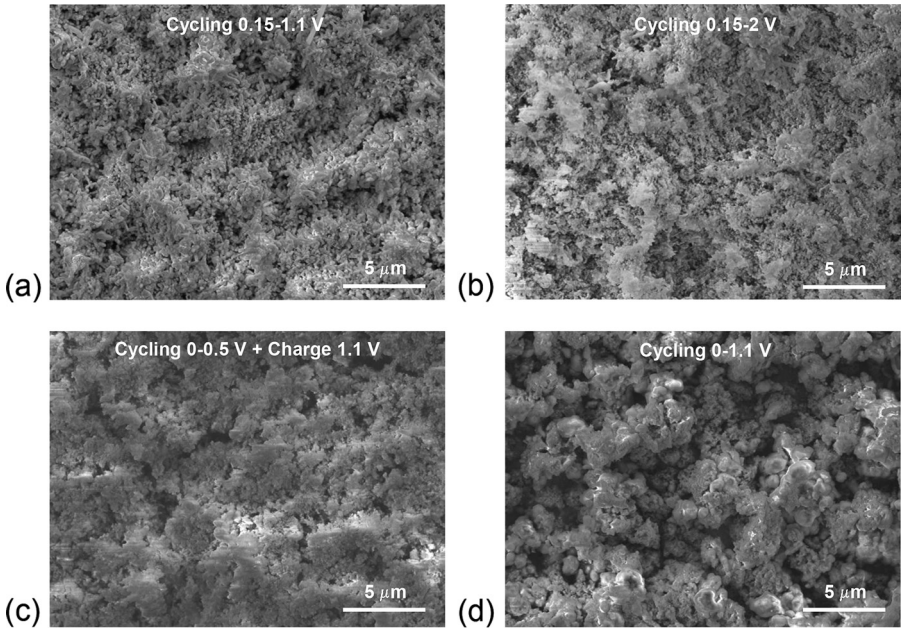

Fig. 14. Morphological properties of cycled indium thin film electrodes measured with SEM. Representative SEM photographs of indium thin film electrodes after cycling with Li from (a) 0.15–1.1 V, (b) 0.15–2 V, (c) 0–0.5 V, and (d) 0–1.1 V, corresponding to the cycled electrodes results presented in Fig. 12a. In the case of the electrode cycled from 0 to 0.5 V, a charge to 1.1 V was applied before SEM inspection.

the repeated (de)insertion electrochemical reaction as profound as for the other electrodes, as suggested by its larger remaining capacity. For the electrode cycled from 0 to 1.1 V (Fig. 14d), the particles are much larger with what appear to be deeper cracks in the surface and are associated with the faster decline in capacity. All electrodes materials show important signs of charging effects, which suggest that the agglomerated masses are not well connected electronically and/or are passivated by significant quantities of insulating products from the SEI. From these results, it is clear that the morphology of the starting films (Fig. 1a) has been significantly altered during repeated cycling, and the effect of applying various cut-off voltages result in the formation of different film morphologies influenced by the specific reaction pathways associated with the cut-off voltages.

4. Conclusions

The electrochemical and structural properties of pure indium thin film anodes have been investigated with respect to Li and Na ion chemistries. The reaction is severely limited by the anomalous electrolyte decomposition if no electrolyte additives are employed. Using 5 wt% FEC suppresses the anomalous side reaction during the first cycle with Li but does not prevent the reaction upon further cycling if conducted from 0 to 2 V. If the reaction is restricted from 0.15 to 2 V or form 0–1.1 V, the anomalous side reaction is suppressed. Based on XPS findings, we attribute the anomalous electrolyte decomposition to the catalytic role of native surface oxides for the pristine electrode cycled without FEC additive. When using 5 wt% FEC, In^{3+} species formed during the cycle at 0–2 V may be responsible for the electrolyte decomposition. Restricting the charge at 1.1 V, limiting the discharge to 0.15 V, or using a larger quantity of FEC effectively suppresses the electrolyte decomposition upon further cycling. For Li-ion batteries, indium anodes offer good storage capacity of 950 mAh g^{-1} associated with the formation of $Li_{13}In_3$, close to the theoretical value of 1012 mAh g^{-1}. The storage capacity for Na-ion batteries is significantly less at 125 mAh g^{-1}, little more than a fourth the theoretical value of 467 mAh g^{-1}. In the case of Li, the indium thin films can deliver high rate capability with nearly 100% of the maximum capacity retrieved at 10 C and more than 75% recovered at 100 C. In the case of Na, moderately good rate capability can be obtained with about 80% of the maximum capacity retained at 30 C.

Acknowledgments

This work was supported by the U.S. Department of Energy (DOE), Basic Energy Sciences (BES), Materials Sciences and Engineering Division. Microscopy research was supported via a user project supported by ORNL's Shared Research Equipment (ShaRE) User Program, which is also supported by DOE-BES.

Appendix A. Supplementary data

Supplementary data related to this article can be found at http://dx.doi.org/10.1016/j.jpowsour.2013.10.033.

References

[1] B.L. Ellis, L.F. Nazar, Curr. Opin. Solid State Mater. Sci. 16 (2012) 168–177.
[2] L. Baggetto, P. Ganesh, R.P. Meisner, R.R. Unocic, J.-C. Jumas, C.A. Bridges, G.M. Veith, J. Power Sources 234 (2013) 48–59.
[3] L.D. Ellis, T.D. Hatchard, M.N. Obrovrac, J. Electrochem. Soc. 159 (2012) A1801–A1805.
[4] L. Baggetto, P. Ganesh, C.-N. Sun, R.P. Meisner, T.A. Zawodzinski, G.M. Veith, J. Mater. Chem. A 1 (2013) 7985–7994.
[5] A. Darwiche, C. Marino, M.T. Sougrati, B. Fraisse, L. Stievano, L. Monconduit, J. Am. Chem. Soc. 134 (2012) 20805–20811.
[6] L. Baggetto, P.H.L. Notten, J. Electrochem. Soc. 156 (2009) A169–A175.
[7] L. Baggetto, J.K. Keum, J.F. Browning, G.M. Veith, Electrochem. Commun. 34 (2013) 41–44.
[8] L. Baggetto, R.A.H. Niessen, F. Roozeboom, P.H.L. Notten, Adv. Funct. Mater. 18 (2008) 1057–1066.
[9] C.-M. Park, J.-H. Kim, H. Kim, H.-J. Sohn, Chem. Soc. Rev. 39 (2010) 3115–3141.
[10] O.I. Malyi, T.L. Tan, S. Manzhos, Appl. Phys. Express 6 (2013) 027301-1–027301-3.
[11] O.I. Malyi, V.V. Kulish, T.L. Tan, S. Manzhos, Nano Energy (2013). http://dx.doi.org/10.1016/j.nanoen.2013.04.007.
[12] L. Baggetto, J.-C. Jumas, J. Górka, C.A. Bridges, G.M. Veith, Phys. Chem. Chem. Phys. 15 (2013) 10885–10894.

[13] L. Baggetto, M. Marszewski, J. Górka, M. Jaroniec, G.M. Veith, J. Power Sources 243 (2013) 699–705.
[14] L. Baggetto, E. Allcorn, A. Manthiram, G.M. Veith, Electrochem. Commun. 27 (2013) 168–171.
[15] L. Baggetto, E. Allcorn, R.R. Unocic, A. Manthiram, G.M. Veith, J. Mater. Chem. A 1 (2013) 11163–11169.
[16] A. Darwiche, M.T. Sougrati, B. Fraisse, L. Stievano, L. Monconduit, Electrochem. Commun. 32 (2013) 18–21.
[17] J. Sangster, A.D. Pelton, J. Phase Equilib. 12 (1991) 37–41.
[18] S.C. Sevov, J.D. Corbett, J. Solid State Chem. 103 (1993) 114–130.
[19] J.T. Vaughey, C.S. Johnson, A.J. Kropf, R. Benedek, M.M. Thackeray, H. Tostmann, T. Sarakonsri, S. Hackney, L. Fransson, K. Edström, J.O. Thomas, J. Power Sources 97–98 (2001) 194–197.
[20] C.J. Wen, R.A. Huggins, Mat. Res. Bull. 15 (1980) 1225–1234.
[21] C.S. Johnson, J.T. Vaughey, M.M. Thackeray, T. Sarakonsri, S.A. Hackney, L. Fransson, K. Edström, J.O. Thomas, Electrochem. Commun. 2 (2000) 596–600.
[22] K.C. Hewitt, L.Y. Beaulieu, J.R. Dahn, J. Electrochem. Soc. 148 (2001) A402–A410.
[23] A.J. Kropf, H. Tostmann, C.S. Johnson, J.T. Vaughey, M.M. Thackeray, Electrochem. Commun. 3 (2001) 244–251.
[24] Wen-Hsien Ho, Ching-Fei Li, Han-Chang Liu, Shiow-Kang Yen, J. Power Sources 175 (2008) 897–902.
[25] Y.-H. Cui, M.-Z. Xue, X.-L. Wang, K. Hu, Z.-W. Fu, Electrochem. Commun. 11 (2009) 1045–1047.
[26] S.D. Beattie, T. Hatchard, A. Bonakdarpour, K.C. Hewitt, J.R. Dahn, J. Electrochem. Soc. 150 (2003) A701–A705.
[27] L. Baggetto, PhD Thesis, Eindhoven University of Technology, The Netherlands, 2010, p. 147.
[28] M. Faur, M. Faur, D.T. Jayne, M. Goradia, C. Goradia, Surf. Interface Anal. 15 (1990) 641–650.
[29] G.E. McGuire, G.K. Schweitzer, T.A. Carlson, Inorg. Chem. 12 (1973) 2450–2453.